VEHICLE DETECTION AND ROADSIDE TREE SHADOW REMOVAL IN HIGH RESOLUTION SATELLITE IMAGES

Siri Øyen Larsen and Arnt-Børre Salberg

Norwegian Computing Center, Section for Earth Observation,
P.O. Box 114 Blindern, NO-0314 Oslo, Norway,
salberg@nr.no

WG IV/4

KEY WORDS: Vechicle detection, pattern recognition, shadow processing, Quickbird

ABSTRACT:

Over the last few years, the increased availability of high resolution remote sensing imagery has opened new opportunities for road traffic monitoring applications. Vehicle detection from satellite images has a potential ability to cover large geographical areas and can provide valuable additional information to traditional ground based counting equipment. However, shadows cast from trees and other vegetation growing along the side of the road cause challenges since it can be confused with dark vehicles during classification. As the intensity properties of dark vehicles and vegetation shadow segments are visually inseparable in the panchromatic image, their separation must be exclusively based on shape and context. We first present a method for extraction of dark regions corresponding to potential shadows by the use of contextual information from a vegetation mask and road vector data. Then we propose an algorithm for separating vehicles from shadows by analyzing the curvature properties of the dark regions. The extracted segments are then carried on to the classification stage of the vehicle detection processing chain. The algorithm is evaluated on Quickbird panchromatic satellite images with 0.6m resolution. The results show that we are able to detected vehicles that are fully connected with the cast shadow, and at the same time ignore false detections from tree shadows. The performance evaluation shows that we are able to obtain a detection rate as high as 94.5%, and a false alarm rate as low as 6%.

1 INTRODUCTION

Traffic statistics is a key parameter for operation and development of road networks. Vehicle counts based on automated satellite image analysis can provide useful additional information to traditional ground based traffic surveillance. A significant advantage of satellite based technology is that it does not require installation and maintenance of equipment in the road. Moreover, a satellite image can cover large geographical areas, as opposed to traditional ground based traffic measurement equipment. Satellite imagery are therefore particularly suitable for creating short term traffic statistics of specific locations.

Several algorithms for vehicle detection in remote sensing have been developed during the last decade. Most of the examples found in the literature use aerial imagery with resolutions in the range 10-30 cm, see e.g., (Hinz, 2005, Holt et al., 2009, Zhao and Nevatia, 2003). Some examples using satellite imagery, where current commercially available sensors have panchromatic resolution as good as 0.5-1.0 m, also exist, e.g., (Jin and Davis, 2007, Zheng and Li, 2007, Pesaresi et al., 2008, Eikvil et al., 2009, Larsen et al., 2009).

We have developed a strategy for automated vehicle detection in very high resolution satellite imagery. Evidently the ideal choice of methods for automatic vehicle detection depends on the conditions in the image, which again depends on location, type of road, traffic density, etc. We have decided to focus on typical Norwegian roads, which are characterized as narrow, curvy, and sparsely trafficated compared to highways in other countries from which published studies exist. Moreover, a frequent problem is that much of the road surface is hidden by shadows from trees along the side of the road. Dark vehicles are particularly difficult to detect along roads where such shadows are present. Often the vehicle is "connected" to the tree shadow, and the gray level pixel intensities do not provide enough information to discriminate the vehicle from the shadow. To solve this problem, we propose a method based on analyzing the border contour of the shadows (with the connected vehicle), and propose criteria based on the curvature and normal vector to localize the vehicle.

The vehicle detection strategy consists of a segmentation stage, where image objects representing vehicle candidates are found, followed by feature extraction and classification. During the segmentation stage (Section 3.3), interesting image features are first located using a scale space filtering approach, which effectively and robustly detects possible vehicle candidates. The spatial extent of the detected objects are then defined using a region growing approach. At this stage of the processing, the objects are analyzed in order to separate tree shadows from dark vehicle objects (Section 3.4). Finally, we perform feature extraction and classification of objects as vehicles or non-vehicles, and derive vehicle counts from the classified image (Section 3.5).

In this work we concentrate on the tree shadow problem as a part of a complete processing chain for the derivation of vehicle counts from satellite images. Thus the stages of the algorithm that are not related to the tree shadow problem will only briefly be explained. The interested reader is referred to (Larsen and Salberg, 2009) for a complete description of the vehicle detection chain.

2 IMAGE AND ANCILLARY DATA

To be able to detect vehicles, satellite images of high resolution are required. In this study we apply six Quickbird satellite images with 0.6m ground resolution in the panchromatic band covering the period from 2002 to 2009.

Geographical information about the location and width of the road are available, and used to define a road mask. However, the

quality of this data was not sufficiently high, and the road mask was drawn manually.

3 METHODS

Before we present the vehicle detection algorithm we provide some background information on curves and spline models that constitute a central part of separating dark vehicles from shadows.

3.1 Tangent, normal vector and curvature of a parametrized curve

Let $\mathbf{c}(\tau) = [x(\tau), y(\tau)]^T$ be a parametrization of a curve. The unit tangent vector is defined as

$$\mathbf{t}(\tau) = \mathbf{v}(\tau)/\|\mathbf{v}(\tau)\| \tag{1}$$

where $\mathbf{v}(\tau) = [x'(\tau), y'(\tau)]^T$ is the derivative of the curve. Now, consider the second derivative $\mathbf{a} = [x''(\tau), y''(\tau)]^T$. This may be decomposed into two components, one that is parallell and one that is orthogonal to $\mathbf{v}(\tau)$, i.e. $\mathbf{a}(\tau) = \mathbf{a}_{||}(\tau) + \mathbf{a}_{\perp}(\tau)$. The parallel component of the projection of $\mathbf{a}(\tau)$ onto $\mathbf{v}(\tau)$ is $\mathbf{a}_{||}(\tau) = a_{||}(\tau)\mathbf{v}(\tau)$, where $a_{||}(\tau) = \mathbf{a}^T(\tau)\mathbf{v}(\tau)/\|\mathbf{v}(\tau)\|^2$. The normal vector $\mathbf{n}(\tau)$ to the parametrized curve is defined as the unit vector in the direction of $\mathbf{a}_{\perp}(\tau)$, i.e.

$$\mathbf{n}(\tau) = [n_x(\tau), n_y(\tau)]^T = \frac{\mathbf{a}_{\perp}(\tau)}{\|\mathbf{a}_{\perp}(\tau)\|}, \tag{2}$$

where

$$\mathbf{a}_{\perp}(\tau) = [x''(\tau), y''(\tau)]^T - \frac{x''(\tau)x'(\tau) + y''(\tau)y'(\tau)}{[x'(\tau)]^2 + [y'(\tau)]^2}[x'(\tau), y'(\tau)]^T. \tag{3}$$

We define the normal direction as

$$\phi_{\mathbf{n}}(\tau) = \tan^{-1}(n_y(\tau)/n_x(\tau)). \tag{4}$$

The signed curvature of the contour measures the rate of change of the tangent (derivative of the tangent with respect to the arc length) and is given as (Nixon and Aguado, 2002)

$$\kappa(\tau) = \frac{\|\mathbf{t}'(\tau)\|}{\|\mathbf{v}\|} = \frac{x'(\tau)y''(\tau) - y'(\tau)x''(\tau)}{([x'(\tau)]^2 + [y'(\tau)]^2)^{3/2}}. \tag{5}$$

Note that the curvature of a circle with radius R is $\kappa(\tau) = 1/R$.

3.2 Thin plate regression splines

Assume that we are given a set of N sample points of a silhouette contour. To create a parametrized representation $\mathbf{c}(\tau)$ of the sample points we will model the components $x(\tau)$ and $y(\tau)$ using a thin plate regression spline (TPRS) (Wood, 2003). The TPRS is a smoothing spline which is beneficial when the curve is estimated from a noisy silhouette contour. At location τ the "smoothed" function $x(\tau)$ (similar for $y(\tau)$) may be expressed as (Green and Silverman, 1994, Wood, 2003)

$$x(\tau) = \sum_{i=1}^{N} \delta_i \eta(|\tau - \tau_i|) + \alpha_1\tau + \alpha_0, \tag{6}$$

where

$$\eta(|\tau|) = \frac{\Gamma(-3/2)}{2^4\pi^{1/2}}|\tau|^3, \tag{7}$$

and N is the number of sample points of the contour. The parameters δ_i and α_j are estimated using the algorithms given in (Wood, 2003). One of the key points in (Wood, 2003) is reduced rank modelling of the estimation problem, in the sense that the smoothed function is constructed by an eigen decomposition and truncation of the solution of the thin plate spline smoothing problem. The obtained basis is optimal in the sense that the truncation is designed to result in the minimum possible perturbation of the thin plate spline smoothing problem for a given bases dimension. The maximum number of degrees of freedom refers to the dimension of the truncated bases. Hence, N variables δ_i, $i = 1, 2, \ldots, N$ may be modelled using only M variables, and the total number of unknowns to estimate is $M + 2$ given by $\boldsymbol{\beta} = [\beta_1, \beta_2, \ldots, \beta_M, \alpha_0, \alpha_1]^T$.

A smoothing parameter λ plays an important role when using thin plate regression splines (Wood, 2003). The smoothing parameter is estimated as the value that minimized the generalized cross-validation (see e.g. (Green and Silverman, 1994)).

Now, the derivative of the TPRS model $x(\tau)$ may easily be calculated as

$$x'(\tau) = \sum_{i=1}^{N} \delta_i \eta'(|\tau - \tau_i|) + \alpha_1, \tag{8}$$

where

$$\eta'(|\tau|) = \text{sign}(\tau)\frac{3\,\Gamma(-3/2)}{2^4\pi^{1/2}}|\tau|^2, \tag{9}$$

and similarly the second derivate

$$x''(\tau) = \sum_{i=1}^{N} \delta_i \eta''(|\tau - \tau_i|) \tag{10}$$

where

$$\eta''(|\tau|) = \frac{6\,\Gamma(-3/2)}{2^4\pi^{1/2}}|\tau|. \tag{11}$$

Note that it is the same parameters δ_i, $i = 1, \ldots, N$, α_1 and α_0 involved in the expressions for $x(\tau)$, $x'(\tau)$ and $x''(\tau)$, and the parameter estimation is performed on an observed (noisy) curve. This is beneficial, since computing the derivative numerically enhances any noise. The TPRS expression for $x(\tau)$ and $y(\tau)$ may now be used to calculate the tangent, the normal vector and the curvature of $\mathbf{c}(\tau)$ analytically at any location τ on the curve.

Since the border contours are closed, we avoid edge effects in $\mathbf{c}(\tau)$ by extending the edges of the contour. Another factor that needs to be determined is M. Here we have chosen M equal to 0.9 times the length of the contour. If M is too small the contour will be over-smoothed, and desirable features will not be captured.

3.3 Extraction of candidate vehicle image objects

Potential vehicles are located in a scale space filtering step. Since vehicles have an elliptical shape in high resolution satellite images, we have extended the scale space circular blob detection approach proposed by Blostein and Ahuja (Blostein and Ahuja, 1989) to the more general approach of detecting elliptical blobs. The image is convolved with an elliptical Laplacian of Gaussian filter

$$\nabla^2 G(x, y; \sigma_x, \sigma_y) = \left(\frac{(\sigma_x^2 - x^2)}{\sigma_x^4} + \frac{\sigma_y^2 - y^2)}{\sigma_y^4}\right) e^{-\left(\frac{x^2}{2\sigma_x^2} + \frac{y^2}{2\sigma_y^2}\right)} \tag{12}$$

at various scales (σ_x, σ_y). At local extrema in the response image, the size and contrast of best fitting ellipses are estimated using analytical expressions for the response of an "ideal" ellipse image to the $\nabla^2 G$ filter in addition to a σ-differentiated Laplacian of Gaussian filter $(\frac{\partial}{\partial\sigma_x} + \frac{\partial}{\partial\sigma_y})\nabla^2 G$. (The second filter

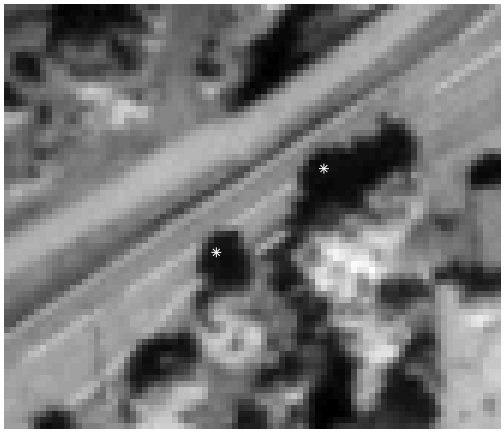

(a)

(b)

Figure 1: White asterisk marks dark blob center, black asterisk mark bright blob center. Only blob centers found within the road mask and passing the size and contrast thresholds are displayed.

is needed since there are two unknowns, i.e., scale and contrast (Blostein and Ahuja, 1989)). Locations at which the estimated scale is close to the scale of the filter, and the estimated contrast is higher than a preset threshold, are treated as points of interest, i.e., as candidate vehicle center locations (Figure 1). Note that the principal direction of the elliptical filter should match the orientation of the road, and hence the vehicles in the image. Thus, the image must be rotated prior to convolution with the filters. Details of the scale space filtering step can be found in (Larsen and Salberg, 2009).

After filtering, we extract the vehicle silhouettes from the list of candidate vehicle centers, i.e., we define the spatial extension of the blob surrounding the blob center. Once we have object silhouettes, we can extract many features describing the objects, and use classification to separate vehicles from non-vehicles. The objects are found using a simple region growing technique, as follows: Start at the pixel closest to the blob center, and grow an object by including all neighbouring pixels that have intensity below/above[1] a given threshold, until no more pixels can be included.

[1]The sign of the Laplacian of Gaussian filter is adjusted so that a local minimum in the convolution response represents a dark blob, while a local maximum represents a bright blob. Naturally, a dark threshold must be used as an upper threshold for the intensities that can be included during region growing of a dark blob, while a bright threshold is used as a lower threshold when growing a bright blob.

3.4 Separation of dark vehicle objects from tree shadows

If we restrict region growing to the road, i.e., if the region is not allowed to grow outside the road mask, we get many tree shadow objects that can easily be confused with dark vehicles (Figure 2). On the other hand, by letting the region grow outside the road, some vehicles would be joined with a tree shadow object (and probably lost during classification), since some dark vehicles appear so close to a tree shadow that the vehicle can not be separated from the shadow based on intensity features alone (Figure 3).

This dilemma can be solved if we look at how the human interpreter recognizes the car in Figure 3, i.e., by looking at the shape, and not just the intensity. While the car has a similar dark gray tone to the tree shadows, the shape of the region reveals that there is a car connected to the tree shadow. Two criteria that can be used to recognize such a shape are related to the transition zone from car to shadow;

- the border contour of the region has strong negative curvature.
- the outward normal vector of the contour points of the region is in the same direction as the road.

These two criteria, form the basis of our algorithm for separating dark vehicles from tree shadows. When growing a region from a dark blob center, we must let the region grow outside the road mask, to see whether it enters a vegetation shadow area. More specifically, we let the region grow outside on the side of the road where vegetation cast shadows are expected to come from. This is determined by the sun angle, which is known at the time of image acquisition. If the resulting region overlap the vegetation shadow both inside and outside the road, we search the border contour of the region for points that meet both the stated criteria. Moreover, if the original region is divided along a line connecting the mentioned points (from now on called "clip points"), and the shape of the resulting sub region inside the road resembles the shape of a vehicle, then this region should be considered a vehicle candidate (Figure 4). Otherwise (if clip points are not found), we assume that the region represents tree shadow only, and ignore it in the further processing of the image. It may be that vehicles are contained in regions were no clip points are found, however, we have no means of distinguishing them from three shadows.

3.4.1 Clip point criteria When an object region consists of both a dark vehicle and tree shadows, we call the border points that mark the transition from vehicle to tree shadow clip points (Figure 4), since they can be used to divide ("clip") the region into its two constituent parts. The border contour is found from the binary image representing the region, using a straight forward contouring algorithm. The extracted contour points are then modelled using the TPRS model described in Sec. 3.2. A clip point τ_c of the TPRS modelled border contour $\mathbf{c}(\tau)$ is defined as a point where

- the curvature $\kappa(\tau_c) < -0.2$ (corresponding to a cirle of $R = 3.0$m), and
- the difference between the (outward or inward) normal direction of the contour and the orientation of the road is less than five degrees, i.e. $|\phi_{\mathbf{n}}(\tau_c) - \theta_r| < 5^o$, where θ_r denotes the direction of the road.

The curvature and angle thresholds were selected based on prior knowledge and trial and error on a few examples.

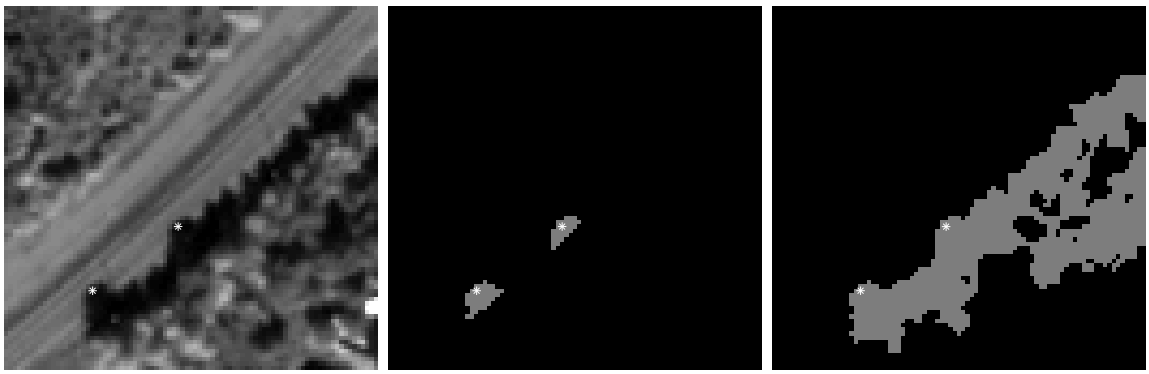

(a) (b) (c)

Figure 2: Tree shadows. White asterisk marks dark blob center. Panchromatic image in (a), and corresponding segment images; in (b), region growing is restricted to the road mask, while in (c), the region is allowed to grow outside the road.

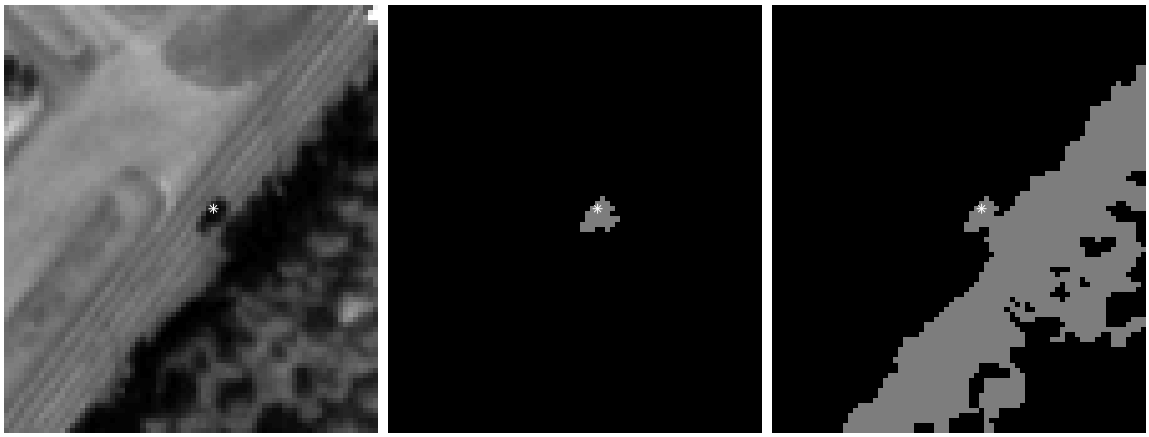

(a) (b) (c)

Figure 3: Car connected to tree shadows. White asterisk marks dark blob center. Panchromatic image in (a), and corresponding segment images; in (b), region growing is restricted to the road mask, while in (c), the region is allowed to grow outside the road.

The contour is traversed in both directions in turn, starting at a point lying inside the road. The traversal stops when:

1. reaching a point lying more than two pixel units (1.2m) outside the road mask,
2. reaching a point outside the road mask for the second time, or
3. reaching a clip point τ_c.

If clip points are found in both directions, some requirements are necessary in to order extract a vehicle candidate from the shadow mask. The region is divided ("clipped") into two constituent parts if:

1. The normal directions of the contour at the two clip points have opposite signs, i.e. $|\phi_{\mathbf{n}}(\tau_{c1}) - \phi_{\mathbf{n}}(\tau_{c2})|$ is between 170 and 190 degrees.
2. The distance between the clip points does not exceed five pixel units (3.0m), i.e. $\|\mathbf{c}(\tau_{c1}) - \mathbf{c}(\tau_{c2})\| < 5$.
3. The resulting vehicle candidate object (i.e., the object that corresponds to the part of the region inside the road after clipping) is a connected region (i.e. it contains only one silhouette).
4. The difference between the orientation of the vehicle θ_v candidate object and the orientation of the road θ_r is less than 45 degrees [2].

Also here the thresholds were selected based on prior knowledge and trial and error on a few case studies.

3.5 Feature extraction and classification

For each image object, we extract a number of features that can be used to separate vehicles from other type of objects. The extracted features include both radiometric, geometric, and context based features. Using branch-and-bound feature selection we found separate optimal feature sets for bright and dark objects. For bright objects, the selected features are

- contrast, elongation, panchromatic intensity, standard deviation, and mean sobel gradient of the region.

For dark objects, the features are

- $\nabla^2 G$ amplitude, contrast in the longitudinal direction, length, area, perimeter, amount of overlap with the road edge, and absolute difference between the angle orientation of the object and the road angle orientation.

[2] The angle of the object is determined from the central moments as $\theta_v = 0.5\tan^{-1}(\mu_{11}/(\mu_{20} - \mu_{02}))$

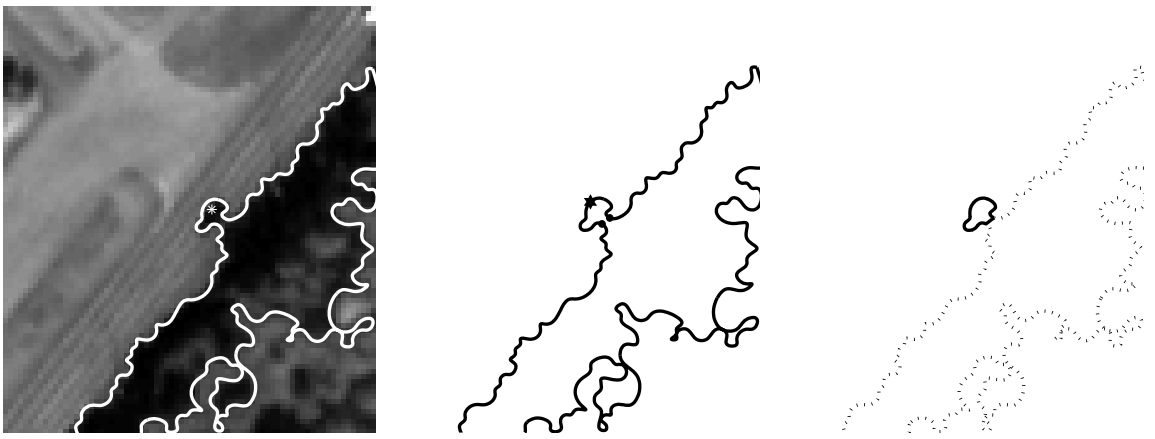

(a) (b) (c)

Figure 4: (a) Same as Figure 3(a), but in addition, a white contour marks the border of the object region initially grown from the blob center. (b) A solid line shows the contour, the star marks the start point for search along the contour, the circles mark points with strongly negative curvature and opposite normal directions, both parallell to the road direction. (c) The dotted line shows the initial contour, while the solid line is the contour of the new region (after clipping).

Classification is performed on bright and dark segments separately. We use a K-nearest-neighbor classifier with $K = 3$. We define two classes - vehicle and non-vehicle. Prior to classification, the mean of the feature space is shifted to the origin, and the features are scaled to unit total variance, neglecting class relationships.

3.5.1 Extraction of vehicle positions The output from the classification is an image in which each object is labeled as vehicle or non-vehicle. Since a vehicle may be represented by more than one object, the classification output images must be processed to check for objects that should be merged. More specifically, a bright vehicle may be represented by a bright and/or a dark object (the vehicle shadow) (Fig. 1(b)). The final image is constructed by adding the two images representing bright and dark objects classified as vehicles. To ensure that bright vehicles are not counted twice (the vehicle object and the shadow object), bright objects are dilated in the direction of the expected shadow, i.e., given the known position of the sun in the sky at the moment of image acquisition, in order to ensure overlap of the objects. The number of detected vehicles is then found by counting the number of final vehicle objects.

4 EXPERIMENTAL RESULTS AND DISCUSSION

The methods were tested on a total of 48 sub scenes from six different satellite images. The scenes contain a total of 182 vehicles (Tab. 1). All the objects were manually labelled as vehicle or non-vehicle. Segments that represent car shadows were considered to belong to the vehicle class, as they share similar geometrical and spectral properties as dark vehicle segments. For classification, testing was performed using one sub scene at the time, leaving the objects from the relevant sub scene out of the training set (leave-one-out approach). The classification error was 0.6% for bright objects and 4.6% for dark objects.

Tab. 1 shows results for each of the six images as a sum of the results from the corresponding sub scenes. The number of vehicles in the table corresponds to the number of vehicles that are visible in the image and found by manual inspection. The segmentation result was manually inspected and compared to the marked vehicle positions. Based on this inspection we found the number of vehicles that were correctly segmented, i.e., all vehicles except those that fail to be segmented or are combined with a non-vehicle object into a joint segment. The number of correctly detected vehicles and the number of false alarams are found by comparing the final vehicle objects (cf. Sec. 3.5.1) to the true vehicles in the image. From this we see that the detection rate, i.e., the fraction of vehicles that are detected, is 94.5%. The false detection rate, i.e., the number of false alarms divided by the number of vehicles, is 6.0%.

Image	Vehicles	Correctly segmented vehicles	Correctly detected vehicles	False alarms
Østerdalen 2004	44	44	43	4
Østerdalen 2009	23	23	23	2
Kr. sund 2004	33	32	30	1
Kr. sund 2008	47	44	42	2
Sollihøgda 2002	9	9	9	0
Sollihøgda 2008	26	26	25	2
Total	182	178	172	11

Table 1: Experimental results

As seen in Tab. 1, the detection rate ranges from 89.4% to 100% among the six images. The performance also vary with the location. For example, all the segmentation errors occurred in the Kristiansund images. These images contain more clutter (e.g., differences in the two road lanes, road surface material patches, lane markings, etc.) than the images from the other locations. The Østerdalen images have more false alarms compared to the number of vehicles than the images from the other two locations. A fair explanation is that the traffic density is lower in Østerdalen. Actually, the average number of false alarms per km is 0.12 in Østerdalen, while it is 0.17 and 0.32 in Kristiansund and Sollihøgda, respectively.

Omission errors occur almost exclusively in cases where the region growing routine fails. In each of these vehicle cases, a blob was located during the filtering step, but the grown object fails to capture the actual shape of the vehicle, hence the object is classified as non-vehicle.

5 SUMMARY AND CONCLUSIONS

We have presented an approach for vehicle detection using very high resolution satellite imagery. We have focused the attention on smaller highways representing typical Norwegian road conditions, i.e., relatively narrow roads, low traffic density and rural areas where roads are often partially covered by tree shadows. The processing chain starts with a panchromatic satellite image and a corresponding road mask, and consists of the steps segmentation, feature extraction and classification.

The proposed segmentation strategy is based on a Laplacian of Gaussian filter which is used to search through the image for elliptically shaped "blobs", i.e., regions of relatively constant intensity that is brighter or darker than the local background. Although this approach is robust towards local contrast changes, and extracts nearly all the vehicle positions in the image, it also finds many candidates representing other kinds of objects.

In particular, shadows pose a special challenge since the intensities of shadowed areas are similar to dark vehicles. However, using our novel apporach only two false alarms are caused by tree shadows - one of which represent a tree shadow region whose shape resembles that of a vehicle. The fact that there are so few errors caused by tree shadows is a significant and important improvement compared to previous results (Larsen et al., 2009). Other false alarms are caused by e.g. vehicle shadows, trailor wagons (counted in addition to the vehicle pulling it), or spots in the road surface.

Compared to our previous study (Larsen et al., 2009), the detection rates have been significantly improved, and may in many cases now be considered acceptable for operational use. The blob detection strategy has proved to be especially useful for this application, since almost all the vehicles in our data set represented a local extremum in the image response to convolution with the elliptical $\nabla^2 G$ filters. However, there are still some aspects that should be adressed. First of all, the approach for handling tree shadows is new, and validation on more data may be needed before it can be used for operational use. Secondly, false alarms due to double count of the same vehicle should be avoided. The vehicles should be classified into groups based on size, e.g., car, van, and truck/bus/trailor wagon. Object regions that are located close to each other must be seen in context to determine whether they belong to the same vehicle. Finally, for operational use, the roads must be automatically localized in the satellite image. The position of the mid line of the road is available as vector data together with rough estimates of road width. However, in order to construct a road mask, these data must be co-registered with the satellite image. As of today, this requires a considerable amount of manual labor. It is therefore necessary to develop algorithms for automatic rectification of the road mask to match the satellite image.

ACKNOWLEDGEMENTS

We thank Line Eikvil, Norwegian Computing Center, for proofreading the manuscript.

REFERENCES

Blostein, D. and Ahuja, N., 1989. A multiscale region detector. Comput. Vis. Graph. Image Process. 45, pp. 22–41.

Eikvil, L., Aurdal, L. and Koren, H., 2009. Classification-based vehicle detection in high-resolution satellite images. ISPRS J. Photogramm. Remote Sens. 64(1), pp. 65–72.

Green, P. J. and Silverman, B. W., 1994. Nonparametric regression and generalized linear models: a roughness penalty approach. Chapman and Hall, London.

Hinz, S., 2005. Detection of vehicles and vehicle queues for road monitoring using high resolution aerial images. In: Proc. 9th World Multiconf. Systemics, Cybern. Informatics, Orlando, Florida.

Holt, A. C., Seto, E. Y. W., Rivard, T. and Gong, P., 2009. Object-based detection and classification of vehicles from high-resolution aerial photography. Photogramm. Eng. Remote Sens. 75(7), pp. 871–880.

Jin, X. and Davis, C. H., 2007. Vehicle detection from high-resolution satellite imagery using morphological shared-weight neural networks. Image and Vision Computing 25(9), pp. 1422–1431.

Larsen, S. O. and Salberg, A. B., 2009. SatTrafikk project report. Technical Report SAMBA/55/09, Norwegian Computing Center, Oslo, Norway. Downloadable from http://publ.nr.no/5190.

Larsen, S. O., Koren, H. and Solberg, R., 2009. Traffic monitoring using very high resolution satellite imagery. Photogramm. Eng. Remote Sens. 75(7), pp. 859–869.

Nixon, M. and Aguado, A., 2002. Feature Extraction & Image Processing. Newnes, Oxford, UK.

Pesaresi, M., Gutjahr, K. and Pagot, E., 2008. Estimating the velocity and direction of moving targets using a single optical vhr satellite sensor image. Int. J. Remote Sens. 29(4), pp. 1221–1228.

Wood, S. N., 2003. Thin plate regression splines. J. R. Statist. Soc. B 65(1), pp. 95–114.

Zhao, T. and Nevatia, R., 2003. Car detection in low resolution aerial images. Image and Vision Computing 21, pp. 693–703.

Zheng, H. and Li, L., 2007. An artificial immune approach for vehicle detection from high resolution space imagery. IJCSNS.